This is a preprint, the final version is subject to change, of the American Mineralogist (MSA)
Cite as Authors (Year) Title. American Mineralogist, in press.
(DOI will not work until issue is live.) DOI: http://dx.doi.org/10.2138/am.2014.4614

Revision 1. Correction date: 8 October 2013

Kaolinite transformation into dickite during burial diagenesis

Javier Cuadros[1*], Raquel Vega[1], Alejandro Toscano[1], and Xabier Arroyo[2]

[1]Department of Earth Sciences, Natural History Museum, Cromwell Road, London SW7 5BD, UK

[2]Faculty of Geological Sciences, Complutense University of Madrid, C/ José Antonio Novais n. 2, Ciudad Universitaria, 28040 Madrid, Spain

ABSTRACT

The mechanism of kaolinite transformation into dickite has been investigating using 13 samples from the Frøy and Rind oil fields (Broad Fourteens basin, North Sea), 3 kaolinite specimens with different crystal order (KGa-2, Kaolinite API 17, Keokuk kaolinite), and 2 dickite-rich samples (Natural History Museum collection). Detailed analysis of XRD, thermal analysis and SEM data show that: (1) as dickite content increases, there is also an increase of the crystal order of kaolinite; (2) in dickite-rich specimens kaolinite and dickite have crystals (or XRD-coherent domains) of the same size; (3) there is no specific dehydroxylation temperature for each polytype, rather particle size and crystal order control dehydroxylation temperature independently of polytype; (4) with progressive dickite content, the development of both particle size and the size of the coherent crystal domains within particles is greater in the c direction than in the ab plane; (5) the growth of defect-free segments in the c direction is not connected with the growth in the a and b directions, as would be expected in crystallization from solution; (6) textural features indicate coalescence of kaolin plates with burial; (7) there is a very weak positive correlation between particle dimensions and relative kaolinite-dickite content. These results are interpreted as resulting from a double reaction taking place in the solid state with burial. Some kaolinite domains grow in size and crystal order while other domains are transformed into dickite. Presumably, also the dickite domains formed early in the transformation grow in crystal order. The transformation into dickite stops at 90-95% dickite because the remaining kaolinite domains are so large and stable that the stability increase produced by the polytype transformation would be negligible.

Keywords: POLYTYPISM: Dickite and Kaolinite, TGA, XRD DATA.

INTRODUCTION

Kaolinite transformation into dickite takes place as a response to increasing temperature in a variety of environments. In the early literature, dickite was related to hydrothermal processes. Zimmerle and Rösch (1990) analyzed dickite occurrences in Europe and concluded that "most of the dickite Phanerozoic sediments of Europe occurs in porous and permeable rocks and is associated with a high degree of coalification, hydrothermal mineralization, and a high present heat flow". According to them, the specific analysis of a large number of sedimentary rock samples within the former German Democratic Republic indicated that increasing age and burial depth alone do not cause kaolinite transformation into dickite. These observations are interesting and helpful to clarify the conditions that trigger or accelerate the transformation, although sufficient evidence has gathered to show that kaolinite-to-dickite transformation takes place frequently in diagenetic conditions. The reaction has been mainly documented in sandstone diagenesis (Shutov et al. 1970; Ehrenberg et al. 1993; McAulay et al. 1994; Lanson et al. 1996; Beaufort et al. 1998; Hassouta et al. 1999; Martin-Martin et al. 2007; De Bona et al. 2008) but also in diagenesis of shale (Ruiz Cruz and Reyes 1998), both sandstone and mudstone (Ruiz Cruz and Moreno Real 1993), and sandstone, siltstone and shale (Marfil et al. 2003). From these studies, it transpires that besides the temperature increment, other factors play a role in facilitating the progress of the reaction. The most important of such factors is water accessibility, which includes porosity and the actual presence of water, as oil in reservoirs appears to stop the transformation (Ruiz Cruz and Moreno Real 1993; Hassouta et al. 1999; Lanson et al. 2002; Marfil et al. 2003; De Bona et al. 2008). Low pH fluids and faulting are also mentioned as favorable factors (Martin-Martin et al. 2007; De Bona et al. 2008).

The present contribution deals with the kaolinite-to-dickite transformation reaction and not with any possible origin of dickite, and thus the focus is on previous literature where kaolinite dickitization is documented by a transformation series. Kaolinite transformation into dicke due to hydrothermal processes is expected and reported occasionally (Parnell et al. 2000), but frequent reports of

hydrothermal dickite do not establish a necessary genetic link between kaolinite and dickite. Choo and Kim (2004) find predominant dickite with mixtures of kaolinite (and also nacrite) that may indicate a kaolinite precursor. Simeone et al. (2005) describe supergene kaolinite and hydrothermal dickite in successive hydrothermal alteration haloes, but without implying a genetic connection between them. Parnell et al. (2004) indicate that two pulses of hot fluids precipitated kaolinite (50-80 ºC) and dickite (maximum 100-120ºC) independently. Dickite of hydrothermal origin is described by Palinkas et al. (2009) as precipitated from fluids (290-330 ºC) possibly derived from K-feldspar and muscovite dissolution. Similarly, dickite of diagenetic origin has been interpreted to form as a result of precipitation from porous solutions in clay-shales (Veniale et al. 2002) mudstones near coal seams (Goemaere 2004) and following partial illite dissolution caused by stress in marls (Buatier et al. 1997).

There is a consistent agreement in the fact that dickite replaces kaolinite, or dickite precipitates preferentially over kaolinite, at a temperature threshold of 80-160 ºC, depending on individual studies. However, studies about the relative stability of the two polytypes do not agree and some of them are at odds with the higher stability of dickite at higher temperatures inferred from natural sequences. Zotov et al. (1998) concluded that kaolinite is metastable with respect to dickite at least up to 350 ºC, and that pressure had a negligible stabilization effect. According to them, the observed prevalence of kaolinite in surface environments and the timing of kaolinite dickitization are due to kinetic effects. De Ligny and Navrotsky (1999), Fialips et al. (2001), and Fialips et al. (2003) determined standard free energies of formation (25 ºC, 1 bar) that were 2-26, 3-8, and 12-25 kJ/mol more stable for kaolinite, respectively. They argued that pressure or temperature would not alter their relative stability. These values would explain that kaolinite is much more abundant than dickite but make kaolinite dickitization problematic. For the latter, they suggest possible explanations such as kinetic factors that affect reaction paths in the polytype precipitation from solution or transformation, and differences in hydration state or minor element chemistry between

kaolinite and dickite that affect their relative stabilities. Calculations of the ΔG of formation at standard conditions (298.15 K and 1 bar) by Anovitz el al. (1991) indicated that kaolinite is more stable than dickite at such conditions by 1.38 kJ/mol, and they argued that the smaller molar volume of dickite may reverse the stability relation at high pressure. Thus, kaolinite dickitization would be driven by pressure. First principle calculations by Sato et al. (2004) produced differences between dickite and kaolinite in the range 0.07-0.3 kJ/mol. Thus, the driving force for dickite replacing kaolinite with increasing temperature remains unknown.

The mechanism of kaolinite dickitization is an essential piece of information to understand the process. It has implications in terms of the driving force, kinetics, and environmental factors promoting or hindering the reaction. The mechanism has been interpreted both as dissolution-precipitation and as a solid-state transformation. A dissolution-precipitation process can possibly have a greater effect on the surrounding sediment by the transient alteration of the fabric during grain dissolution, which would facilitate fluid mobility and Si mobilization.

Support for a solid-state transformation process has been found in several features of the kaolinite-dickite series. The displacement in the frequency of the infrared (IR) OH stretching bands was interpreted by Brindley et al. (1986) to indicate a transition from kaolinite to disordered kaolinite, then to disordered dickite and finally to well-crystallized dickite, consistent with a model of crystal disorder based on displacement of the octahedral vacancies in the layer sequence (all kaolinite layers have the octahedral vacancy in the same position, whereas in dickite the vacancy alternates between the two octahedra at both sides of the crystallographic mirror plane; Bailey 1980). In other words, they suggested that the polytype transition takes place by the displacement of the octahedral occupancy within the crystals as such a mechanism would generate the above-mentioned sequence. Interestingly, Shutov et al. (1970) also found that disordering of kaolinite crystals is a previous step for dickitization. They proposed a model in which kaolinite layers first slide to generate a dickite-

like two-layer sequence and then the cation vacancy is displaced, resulting in a true dickite structure. Such changes would generate dickite domains that then would spread in opposite directions within the kaolinite crystals. Ruiz Cruz and Moreno Real (1993) interpreted the existence of an intermediate structure (perhaps mixed-layer kaolinite-dickite) as indicated by band displacements in their IR spectra, a dehydroxylation event at intermediate position between those typical of the two polytypes (differential thermal analysis, DTA), XRD peak shifts, and possible XRD superlattice peaks. Lanson et al. (1996) interpreted their thermal analysis results and the lack of relation between kaolin grain morphology and polytype also as the transformation via some intermediate structure. Parnell et al. (2000) found that isotope analysis of dickite yields an unrealistically low formation temperature, that suggests transformation from a kaolinite precursor where oxygen is preserved and hydrogen partially exchanged with interstitial water. Franks et al. (1997) found no resetting of the original kaolinite O isotope signature during the transformation to dickite in Algerian sandstone. Among the above features supporting a solid-state transformation, the dehydroxylation event at intermediate temperature between kaolinite (typically ~550 ºC) and dickite (typically ~650 ºC) is inconclusive because (1) highly crystalline kaolinite dehydroxylates at temperatures similar to dickite (Stoch and Wacławska 1981; Suitch 1986), (2) dickite intercalation followed by expulsion of the intercalate reduced dickite dehydroxylation temperature from 660 to 562 ºC, suggesting that dehydroxylation temperature in this range is a function of crystal order and not an intrinsic feature of the polytype structure (Wada 1965), and (3) kaolin particle size has been reported to have some control on dehydroxylation temperature (Beaufort et al. 1998).

It can be expected that solid-state transformation would generate domains of both kaolinite and dickite within mineral grains and crystals and, in principle, the existence of such domains would support this mechanism. Intracrystalline domains of both polytypes were not found in a HRTEM study of sedimentary kaolinite-dickite (Kogure and Inoue 2005a) but were found in a similar study of hydrothermal kaolin (mainly dickite; Kogure and Inoue 2005b), where both kaolinite and dickite

145 domains were present within dickite and kaolinite crystals, respectively. However, the authors
146 interpreted these intracrystal domains as defects in crystal spiral growth from solution. Dickite- and
147 nacrite-like fragments have also been found by HRTEM, selected area electron diffraction, and IR
148 spectroscopy in a sedimentary kaolinite (Johnston et al. 2008; Kogure et al. 2010), where no
149 polytype transformation is likely, which strongly suggests that such fragments are the result of
150 stacking faults. Thus, domains of a different polytype may be frequent in the minerals of the kaolin
151 group simply due to "errors" in the crystal growth, with no connection to a polytype transformation
152 history. Polytype identification of kaolin minerals with electron microscopy techniques is difficult
153 due to fast damage from the electron beam, which delays accumulation of this type of information.
154 Also, these techniques are likely to produce biased results towards highly perfect crystals, more
155 resistant to the ion beam, where domain intercalation might be less abundant or of a different nature
156 than in less perfect crystals.
157
158 The dissolution-precipitation mechanism is most frequently concluded on the basis of the
159 morphological change from vermicular structures, where kaolinite dominates, to blocky crystals
160 where the major component is dickite (Ehrenberg et al. 1993; Beaufort et al. 1998; Hassouta et al.
161 1999; Martin-Martin et al. 2007). However, there is ample evidence that these morphological types
162 are not univocally related to the polytypes, and there exist both vermicular dickite (Lanson et al.
163 1996; Ruiz Cruz and Reyes 1998; Choo and Kim 2004; De Bona et al. 2008) and blocky kaolinite
164 (Ehrenberg et al. 1993; Kumeda et al. 2007). Beaufort et al. (1998) proposed a dissolution-
165 precipitation model including precipitation on large kaolinite grains acting as templates, which
166 would explain the existence of polytypes with both morphologies.
167
168 This contribution is an investigation of the mechanism of kaolinite dickitization in a sandstone
169 sedimentary series from the North Sea by a detailed structural and morphological analysis of the
170 kaolinite-dickite series together with kaolinite end-members and dickite-rich specimens of various

171 characteristics, used for comparison. Crystal growth patterns and textural features are interpreted to
172 indicate a solid-state transformation mechanism.
173
174 **MATERIALS AND METHODS**
175 **Samples**
176 A series of kaolinite-dickite core specimens of diagenetic origin from sandstones in the Frøy and
177 Rind oil fields, Broad Fourteens basin, Brent Formation of the Norwegian Continental Shelf, North
178 Sea, was analyzed (ELK series; Cassagnabere 1998). They were made available by C. Fialips
179 (Total, Pau, France) and D. Beaufort (HydrASA Laboratory, University of Poitiers, France), and
180 were studied as received. They are the 5-10 μm size fraction of specimens from depths 3,036-4,520
181 m. The original samples had been gently dry-ground to less than 2 mm grain size, dispersed in a
182 water suspension by ultrasonic treatment, separated by sedimentation, and hydrocarbons were
183 removed by Soxlhet extraction using chloroform (Cassagnabere 1998). The locality, geological
184 conditions and possibly some of these samples have been described by Lanson et al. (1996) and
185 Beaufort et al. (1998) and the reader is referred to these publications. Specimens from the same
186 locality have been studied by Kogure and Inoue (2005) and Kogure et al. (2005) using several
187 electron microscopy techniques. The original sediments are of aeolian origin. Kaolinite formed after
188 K-feldspar dissolution and then transformed to dickite with increasing burial depth. Maximum
189 burial temperatures experienced by the sediments range from ~110 to <160 ºC (Lanson et al. 1996;
190 Beaufort et al. 1998).
191
192 Three kaolinite and two dickite samples were also studied as a reference for the structural
193 parameters determined in this investigation. 1) The kaolinite KGa-2, from Warren County, Georgia,
194 USA, is of supergenic origin, product of a complex alteration history and has low crystallinity. Its
195 geological context is described by Moll (2001). It was provided by the Source Clays Repository of
196 the Clay Minerals Society. The sample was simply ground as provided. 2) The kaolinite API 17

(labeled here as Kaol 17) from Lewistown, Montana, USA, is one of the reference materials from the American Petroleum Institute Project 49. It originated by hydrothermal alteration of feldspar in a syenite porphyry. The geological description can be found in Kerr and Kulp (1949), where this specimen was originally described as dickite, although it was later demonstrated to be kaolinite (Lindberg and Smith 1974). This kaolinite is of intermediate crystallinity. The kaolinite provided by the American Project Institute, which has the appearance of white, soft grains of 0.5-1 cm size, was gently ground, without any further treatment. 3) The Keokuk kaolinite (here labeled as Keokuk) is a very high crystallinity specimen from geodes originated in Keokuk, Iowa, USA. The processes that produced the Keokuk geodes are described by Hayes (1936) as far as they are understood. The accepted interpretation is that kaolinite precipitated in voids produced by carbonate dissolution, from fluids generated after silicate mineral dissolution. There is no reference in this interpretation to hydrothermal activity. Kaolinite from some of the snow-white patches in one of the geodes was scratched with a needle and then gently ground. No further treatment was applied.

The two dickites are from the collection in the Natural History Museum (London). 1) Dickite BM 1927, 60 (here labeled BM 1927) is from a massive slate collected in Kolno, Nowa Ruda, Silesia, Poland. The sample was collected in the first quarter of the XXth century, when this region was part of the Prussian Silesia. Zimmerle and Rösch (1990) indicate that dickite in this area is connected to hydrothermal activity. Some material from the slate was scratched with a needle and gently ground, without any further treatment. 2) Dickite BM 1923, 393 (henceforth BM 1923) is from Red Mountain, San Juan County, Colorado, USA. No more information is available. The specimen consisted of sub-millimeter crystals, of which an aliquot was collected and gently ground.

X-ray diffraction

The samples were analyzed using XRD on random powders. To avoid orientation of the crystals, the samples were side-loaded. Two types of holders were used depending on the amount of sample

223 available. The larger holders produced a more random orientation as observed by the intensity ratio
224 of basal to non-basal reflections. However, only two samples were analyzed in the larger holders,
225 Keokuk and Kaol 17. The analyses were carried out using a Philips PW 1830 diffractometer at 42
226 kV and 42 mA, with Cu Kα radiation, graphite secondary monochromator, 1º divergent slit and 0.1
227 mm receiving slit. The scans were performed between 5 and 80 º2θ, with 0.02 º2θ steps and 8 s of
228 count time per step.
229
230 Several types of analysis were performed using the XRD data. First, mineral phases were identified,
231 including kaolin polytypes (kaolinite, dickite) and non-kaolin phases. The identification of the
232 kaolin polytypes was carried out using the data from Bailey (1980). Second, intensity ratios of non-
233 basal to basal reflections were carried out measuring the height of the 00*l* peaks at 7.15 and 3.57 Å,
234 and *hkl* peaks at 4.45, 2.56 and 1.488 Å, and using the formula
235 $$100 \times h_{\text{non-basal}} / [(h_{7.15\text{Å}} + h_{3.57\text{Å}})/2] \qquad \text{(Eq. 1)}$$
236 where *h* represents peak height. Heights were measured from the line of zero counts, which is a
237 good approximation as the peak heights ranged from 1,000 to 85,000 counts (only two peaks had
238 500 and 600 counts) and the background had 150-250 counts.
239
240 The relative proportion of kaolinite and dickite in the specimens was calculated measuring the
241 intensity of kaolinite and dickite peaks, or groups of peaks, in near proximity. Eleven groups were
242 used (figures in Å and polytype indicated in parenthesis): 1) 3.954 (d), 3.841 (k), 3.791 (d), 3.741
243 (k); 2) 3.428 (d), 3.372 (k); 3) 2.794 (d), 2.753 (k); 4) 2.526 (k), 2.505 (d); 5) 2.386 (d), 2.379 (k);
244 6) 2.340 (k), 2.324 (d), 2.290 (k); 7) 1.989 (k), 1.974 (d); 8) 1.790 (d), 1.781 (k); 9) 1.557 (d), 1.542
245 (k); 10) 1.375 (d), 1.338 (k); 11) 1.318 (d), 1.305 (k). Not all peaks or groups could be used in every
246 specimen due to interference with other mineral phases or because the peak resolution was not
247 sufficient. Particularly, group 5) above could only be used in the BM 1923 and 1927 specimens.
248 The intensities were measured as peak areas by curve-fitting assuming Gaussian shapes, using the

249 package GRAMS/AI from Thermo Galactic. Only curve-fitting calculations that could be
250 reproduced were used. The peak areas within each group were corrected using the experimental
251 peak intensities provided by Bailey (1980) and transformed into polytype percents. In two cases
252 (2.340 and 1.989 Å, both kaolinite) the peaks contain two unresolved reflections which, however,
253 result in an evident widening of the peaks. We assumed that the intensities in Bailey (1980) are
254 heights rather than areas. The overlapping peaks described above would result in a compound peak
255 whose area is the sum of both areas of the two peaks, but with a height that is not the sum of both
256 heights, which would make the peak intensities by Bailey (1980) not applicable to our data. This
257 problem was "corrected" by using half of the measured area in these two cases. The approximation
258 improved the similarity of the calculated polytype percents with those from other peak groups. The
259 polytype percents calculated for each sample were then compared, spurious values were eliminated
260 (one or two values outside the standard deviation of, at least, 4 other values), and the selected values
261 were averaged.
262
263 The XRD patterns were also used to analyze the size of the coherent scattering domains (CSDS) in
264 several directions of the crystals by means of measuring the width at half height of peaks
265 corresponding to different crystal indexes. It was intended to make measurements on peaks
266 corresponding to several 00*l*, 0*k*0, *h*00, 0*kl*, *h*0*l*, *hk*0, and *hkl* indexes (where h, k, $l \neq 0$), however it
267 was not possible in many cases due to large peak overlap. If the peaks were entirely free from
268 overlapping, the measurements were carried out using the integration function of the package
269 GRAMS/AI from Thermo Galactic, in which the background is automatically selected and the
270 measurement performed on the experimental trace. Tests of manual measurements of several peaks
271 confirmed that the background subtraction was correct. If there was moderate overlap between
272 peaks, they were modeled by peak-fitting using the same computer package. Some measurements
273 correspond to composite peaks of both kaolinite and dickite, because they are almost coincident and
274 cannot be resolved. At intermediate and high º2θ values the $K\alpha_1$ and $K\alpha_2$ components were resolved

and the $K\alpha_2$ component was subtracted before the width measurement. The CSDS values were calculated from the measured widths using the Scherrer equation. Similar measurements were carried out on the 00*l* peaks at ¼ and ¾ of the peak height to analyze the existence of two CSDS populations. Small CSDS generate low, wide peaks, whereas large CSDS generate sharp, high peaks. Thus, the lower part of a peak is mainly influenced by the small domains and the higher part by the large domains.

Thermogravimetry

The specimens were thermogravimetrically (TG) analyzed using a TA SDT Q600 apparatus. Ten to 20 mg of sample were analysed on Pt crucibles, using an empty Pt crucible as a reference, between room temperature and 1000 ºC, at a 10 ºC/min rate, and with a nitrogen flow of 10 ml/min. The derivative of the TG curve (DTG) was used for the analysis as results are visually more clear and can be studied with greater resolution. In the temperature range of kaolinite/dickite dehydroxylation (400-800 ºC), the DTG curves consisted of complex systems with several maxima and shoulders. They were decomposed into individual components using the package GRAMS/AI from Thermo Galactic. DTG curves of dehydroxylation events are frequently not symmetric due to kinetic effects, even in perfectly homogeneous samples. However, we assumed Gaussian peaks for the individual components, with the goal of calculating and comparing the area under the DTG curve in several ranges of temperature. The DTG curves of the kaolinite-dickite series from the North Sea displayed similar characteristics and their components were centered roughly at the same temperature. The other samples had very different DTG curves and in most cases the components had their centre at temperatures other than those of the North Sea specimens.

Scanning electron miscroscopy

Five selected samples covering the range of kaolinite-dickite in the ELK series, as well as Keokuk, Kaol 17 and BM 1927 were studied by scanning electron microscopy (SEM), using a JEOL JSM-

820 electron microscope working at 20 kV, with a resolution of 35 Å. Secondary electron and backscattering detectors were used. EDX chemical analysis was used to ascertain the nature of the investigated particles. SEM observations were carried out on powder placed on conductive carbon tape that was attached to the sample holders. The samples were sputter-coated with gold.

The dimensions of 4,638 particles were measured to investigate changes in the particle size during the kaolinite-to-dickite transformation. The number of particles measured for individual samples ranged from 376 (ELK 33) to 1,033 (Keokuk) and was 437-672 particles for the other samples. Measurements were carried out only on particles were the ab plane was discernible from the c direction. Measurements correspond to the c direction, or thickness of the particles, and to two perpendicular dimensions in the ab plane. The largest dimension in the ab plane was labeled long a-b dimension, and the dimension perpendicular to it was labeled short a-b dimension. Typically only two dimensions could be measured in a particle. In very few cases the particle was so placed that the three dimensions could be measured without great error due to perspective. On many occasions only one dimension could be measured.

RESULTS

Kaolinite-dickite quantification using XRD

The studied samples consisted mainly of kaolinite and dickite, with other phases present only in minor amounts. The two XRD patterns where non-kaolin phases were more abundant are shown in Figure 1a,b. All the other samples had a lower level of contamination. Kaolin polytype quantification in samples from the North Sea shows a progressive dickite increase with depth up to a maximum of 94 % dickite (Figure 2). The trend of increasing dickite is in agreement with some previously reported data. For example, Ehrenberg et al. (1993) locate the transition from kaolinite- to dickite-dominated specimens at 2,800-3,200 m in sandstones from the Norwegian continental shelf, similar to our samples. Beaufort et al. (1998) report a change of dickite proportion from 20 to

100 % between 3,000 and 5,000 m in samples from the same Broad Fourteens basin based on IR rather than XRD analysis. However, Lanson et al. (2002) show that the relative proportion of kaolin polytype in sandstones at similar depth is very variable from well to well and not only dependent on the experienced temperature, but also of rock porosity and, possibly, the nature of the interstitial fluid (water or oil). Also based on IR methods, Cassagnabere (1998) and Lanson et al. (2002) show that a few samples were completely transformed into kaolinite at depths ~2,100 m (Frøy reservoir) and ~3,500 m (Rind reservoir).

Our study shows also variability of kaolinite-dickite proportion (Fig. 2) at 3,200-3,500 m depth, where most of the samples come from. However, the data support a reaction path which progresses much between 2,800 and 3,300 m, then the progress is reduced up to 3,600 m where it stops, not reaching completion. The reaction progress was modeled using the equation:

$$\%D = \frac{\%D_{\max}}{1+e^{b(d-c)}} \qquad \text{(Eq. 2)}$$

where *%D* is the dickite percent, $\%D_{max}$ (92.59% in the fitted equation) is the maximum dickite content found, *b* (-0.0097) is the slope, *d* is depth, and *c* (3,055.11 m) is the depth at which the inflexion point occurs in the equation, or the centre in the steep part of the curve. This equation assumes the shape of the transformation progress at shallow depths, and the results is reasonable because the reaction is expected to progress slowly at the beginning, due to the low temperature, and to accelerate as the temperature increases. The model indicates that the transformation begins at 2,500 m. There are no detailed temperature data available for this well and the specific onset temperature can only be roughly assessed. Considering the maximum temperature of ~110 to <160 ºC (Lanson et al. 1996; Beaufort et al. 1998) for the well, assuming that the maximum temperature and burial of 20 ºC and 670 m from the Aquitan Basin (France; Beaufort et al. 1998) is applicable to the studied well, and assuming also a linear temperature gradient, the maximum temperature at 2,500 m would range between 76 and 104 ºC. It is quite interesting that the deepest sample, from almost 1,000 m below the next above it, shows no further development of the transformation

353 reaction. A number of reasons related to environmental factors in the sandstone reservoir may be
354 the cause for this, as indicated above. However, two samples of completely different origin selected
355 as dickite end-members for comparison (BM specimens, Table 1) have in fact a kaolinite
356 component and their composition is similar to the deepest ELK samples. Further to this, two other
357 samples from the Natural History Museum collection, of completely unrelated origin, also
358 considered originally as dickite end-members, are in fact kaolinite-dickite-nacrite, with respective
359 relative proportions 3-70-27 and 6-48-46%. In all cases some proportion of kaolinite exists, even in
360 those samples that experienced conditions that generated a substantial proportion of nacrite. The
361 existence of kaolinite in all cases may indicate that it is intrinsically related to the transformation or
362 formation process rather than to environmental factors, as discussed below. The samples containing
363 nacrite were investigated using XRD as indicated above for the kaolinite-dickite samples, but were
364 not used for the present study because of their significant nacrite content.
365
366 **Measurement of the size of XRD coherent scattering domains**
367 The relative intensity (measured as peak height) of the non-basal to basal peaks decreased with
368 increasing dickite in all the samples studied, as shown in Figure 3a for three different non-basal
369 diffraction peaks. The kaolinite samples show a large dispersion of the relative intensity data. The
370 reason for this dispersion is the large range of crystal order covered by the three kaolinite samples.
371 This was corroborated by plotting the non-basal to basal intensity ratios versus the CSDS of the 001
372 peak (Fig. 3b). It becomes evident that the relative intensity of non-basal to basal diffraction peaks
373 correlates negatively with the CSDS of the basal 001 reflection. The interpretation to this fact is
374 that, across all samples with different origin, from kaolinite to 94 % dickite, the CSDS in the c
375 direction is always larger than in the other crystallographic directions, and progressively so as the
376 crystal order increases. Such fact is not uniquely related to kaolinite-dickite proportion. It is related
377 to the crystal perfection of the kaolin, whether it is kaolinite or dickite (Fig. 3b). The possibility of a
378 preferred orientation effect is discarded because the side-loading procedure produces good random

preparations and because it was tested loading the samples in different wells. Deeper wells produced a more random orientation of the particles (see methods), however, this effect was much smaller than the differences of non-basal to basal ratios observed between samples. As the CSDS grows, the diffracted intensity is gathered in a narrower 2θ angle and thus the peak intensity is higher. Because the CSDS in the c direction is progressively larger than those in the other directions, the relative intensity of hkl to *00l* peaks decreases progressively. We checked whether Fig. 3b introduces a forced correlation because the dependent and independent variables are linked through proportionality between the intensity (height) of the peaks 001 and 002, and their CSDS. However, although some broad positive link between them exists, the correlation is very low (R^2 = 0.3, not shown), indicating that the correlation in Fig. 3b is genuine.

The above result, although not uniquely related to the process of kaolinite transformation into dickite, is relevant to the mechanism of this process, because there is an increase of CSDS during the transformation reaction. It is of interest, then, to examine the progression of the growth of CSDS's in several crystallographic directions. CSDS's were measured for multiple peaks in all samples. For those peaks for which CSDS measurements could be done in the entire range of kaolinite-dickite composition, a small majority displayed a broad positive correlation between dickite content and CSDS (not shown). The others did not show any clear relationship between these two variables. The scatter of CSDS at the kaolinite end was mainly due to the very different crystal order of the samples used. In any case, there was evident scatter in all samples, which was generated by the error involved in the measurement of peak widths. The CSDS of BM samples appeared always within the ranges for the ELK samples with similar dickite content. Given this situation, the analysis of CSDS values was simplified to analyze only the two ends of the kaolinite-dickite series. Only one kaolinite sample was selected as representative of the possible crystal order of the original kaolinite in the North Sea series. The selected kaolinite was Kaol 17 for the following reasons. Keokuk kaolinite is an extraordinary specimen with the highest degree of crystal

perfection ever reported and thus was discarded. KGa-2 is at the other end of the spectrum of crystal perfection and thus possibly not appropriate. Plots of CSDS values versus dickite content showed that Kaol 17 was typically more within the trend (assumed approximately linear) generated by the samples with 42-94% dickite (not shown). Keokuk and KGa-2 appeared above and below this trend, respectively, whether clearly off or near it. For the dickite-rich end, we used those samples with >80% kaolinite. As the two BM samples were indistinguishable from the ELK samples, we used the BM samples also, in order to increase the number of available measurements and improve the statistics.

The results of the analysis are displayed in the experimental section of Table 2. Some of the selected peaks are affected by other coincident reflections, what is probably reflected in the standard deviations of the measurements. Overall, however, the results are meaningful and consistent, which indicates that the peak intensities are dominated by the reflections indicated on Table 2. Each individual value is the average of the number of data indicated in the fourth column. Additionally, the CSDS of the *00l* and *0k0* reflections were also averaged from the results shown above the corresponding averaged values in Table 2. These values were averaged because they included reflections contained within the same plane and thus directly comparable. The CSDS values obtained from the 001 peaks, where kaolinite and dickite reflections could not be deconvolved (K+D) is significantly smaller than CSDS values measured on *00l* deconvolved peaks (K and D values), indicating that there is a widening of the 001 peak due to the overlap of the kaolinite and dickite peaks. Thus the K+D measurement is not accurate.

A very important result of this analysis is that both kaolinite and dickite CSDS's increase with burial. Kaolinite is not merely being transformed into dickite but it also recrystallizes into crystals with fewer defects. The second piece of information that can be extracted from Table 2 is that the growth in crystal perfection is larger in the c direction than in any other direction, and this confirms

the results from Figure 3. The growth measured for the *00l* peaks is 148-163% (the K+D measurement is not considered for the reason given above), approximately twice as much as the growth measured from 0k0 peaks (67-89%) and several times larger than the growth measured from 0kl and hkl peaks (30-51%). In the latter group, there are two values outside the general range, corresponding to growths of 137 and 8%. Most probably, there is an error in the CSDS measurement of $K_{initial}$ in both cases, as there is only one measurement available and the corresponding values are clearly below and above similar CSDS $K_{initial}$ values in the table.

Calculations were performed in order to investigate further the mode of growth of the CSDS in several crystallographic directions. The question asked was: do the measured CSDS's correspond to a homogeneous growth of the coherent structure in every direction? We used the experimental CSDS corresponding to individual dimensions a, b and c to calculate the corresponding dimension of the vectors ab, bc, and abc. This calculation assumes that the CSDS grows homogeneously in every direction. We simplified the data to facilitate the trigonometric calculations. The ab angle (γ), 89.9º in kaolinite and dickite, was made 90º. The bc angle (α), 91.6º in both polytypes, was made also 90º. The ac angle (β), 104.8º in kaolinite and 103.6º in dickite, was made 104º. The results show that the calculated ab dimension (512 Å) is similar to the experimental values (results from peaks 110 and 130). However, the calculated bc and abc dimensions are roughly twice those measured (results from 0kl and hkl peaks). This means that the development of the CSDS is homogeneous in the ab plane, but not in any plane including c. In other words, there exist crystallographic defects within the volume contained by the average experimental defect-free distances measured separately in the a, b and c directions.

Thermogravimetry

The TG and DTG diagrams were entirely dominated by the dehydroxylation features of the kaolin polytypes (Fig. 4) although some other phases were apparent in some of the samples. The North Sea

457 series show a broad dehydroxylation event covering the temperature range 450-800 ºC. There is a
458 first event with a broader maximum followed by two other sharp maxima (Fig. 4e-h). The kaolinite
459 samples displayed dehydroxylation events with maxima that were displaced towards higher
460 temperature as the crystal order of the sample increased. For KGa-2 and Kaol 17, the DTG curves
461 were approximately symmetric and their maxima were located in the recognized region for kaolinite
462 (500-550 ºC; Fig. 4a-b). For Keokuk, the DTG shape was complex, starting at 500 ºC and having
463 the main component within the range 600-700 ºC (Fig. 4c), which is typical of dickite. In fact, the
464 Keokuk TG-DTG patterns are similar to those of BM 1927, which contains 89% dickite (Fig. 4d).
465 According to these results, there is not a characteristic dehydroxylation temperature for kaolinite
466 and dickite as such. Rather, the dehydroxylation temperature depends on the crystalline order of the
467 specific specimen. The three kaolinite samples show a progressive widening of the dehydroxylation
468 event and displacement of its center of gravity towards higher temperature as the crystallinity
469 increases. This behavior is consistent with an increasing proportion of well-crystallized particles or
470 domains within particles, although low-crystallinity domains remain (low-temperature side of the
471 dehydroxylation event; Fig. 4a-c). BM 1927 behaves similarly, although it consists mainly of
472 dickite.
473
474 The results from the North Sea series should be interpreted in the same way. With increasing depth,
475 the crystal order of the samples increases and generates crystal domains in which dehydroxylation
476 takes place at increasingly higher temperature, whether these domains correspond to one or the
477 other polytype. This result is in agreement with the XRD data indicating that the crystal order of
478 kaolinite increases with depth, at the same time that it is transformed into dickite.
479
480 The DTG diagrams were decomposed into individual Gaussians to locate approximately the
481 position of the dehydroxylation events of the several crystallographic domains (Fig. 5). The
482 decomposition also allows quantification of the hydroxyl loss within different temperature ranges

(sum of area under the individual components in this range). We investigated the connection of the dehydroxylation temperature with the crystal perfection of the samples. For this, we considered that, approximately, the individual components with their maximum < 550 ºC would correspond to "low crystallinity" kaolin (whether kaolinite of dickite), and those with their maximum > 550 ºC to well crystallized kaolin. There is a good correlation between the sum of the normalized areas of peaks > 550 ºC and the CSDS along the c direction as measured from the 001 peaks (Fig. 6a), which confirms that high-temperature dehydroxylation corresponds to higher crystal order. Keokuk kaolinite plots marginally away from this correlation (Fig. 6a). This analysis correlates the average crystal order as determined by XRD and the portion of sample with high crystal order as indicated by TG. A slightly different approach is to investigate the specific contribution of the well-(or poorly-) crystallized domains to the shape of XRD peaks. The existence of large and small coherent scattering domains in a phase generates peaks which are wide at the base and sharp at the top, because the small domains contribute mainly to the bottom of the peak and thus the large domains have a greater influence in shaping the top of the peaks. We measured the width of the 001 peaks at the lower quarter of their height, where the influence of the small crystal domains would be greatest and then calculated the corresponding CSDS. The correlation of the measured sizes with the area of the DTG dehydroxylation peaks below 550 ºC is good (Fig. 6b), and in this case Keokuk plots closer to the general trend.

SEM

The SEM study of the several samples showed similar morphology for all of them, dominated by plates that had either irregular shape or a regular shape with well defined hexagonal symmetry (Fig. 7). BM 1927 was most different, with large, thick particles of irregular shape consisting of many smaller particles in which it was sometimes impossible to identify the c direction because all dimensions were similar (Fig. 7f). Booklets of plates were frequent in all samples. We searched for possible evidence of growth from solution or particle coalescence. Signs of coalescence were most

frequent. Some of the plates forming booklets appeared to coalesce into one at certain points, mainly at the contact of their basal surfaces (Fig. 7a,b,d,e,f,g) but also laterally (Fig. 7b,e). The sequence of photographs in Figure 7 shows a possible path of plate coalescence in which the particles become thicker and their edges smoother, perhaps tending towards a particle morphology like that in Figure 7g. This path would not be homogeneous because all samples showed very variable particle arrangements and plate thickness. There were also particle aggregates that suggested growth from solution because of the continuity between the sides of the several particles, perhaps indicating growth steps (Fig. 7c), but they were not frequent. Some particles had blocky, rather than plate, morphology (some instances in Fig. 7b, left, and Fig.7g, right). The abundance of these particles did not appear to be related to dickite content.

The quantitative analysis of the evolution of particle dimensions with dickite content is a more robust method to investigate possible transformation mechanisms than the simple observation. This analysis showed that there is no correlation or a very week positive correlation between particle dimensions and dickite content in the North Sea samples (Fig. 8). Keokuk and BM 1927 have dimensions that are within the range of the ELK series, except the average thickness in BM 1927, and only Kaol 17 has dimensions which are consitently smaller. The shape of the particle size diagrams (frequency versus size; not shown) did not progress consistently with average particle size. One would expect that the samples with smaller average size would have sharp distributions, with a great concentration of the frequent sizes, and that larger average sizes would correspond to broader distributions. Such a transition is only apparent between Kaol 17 and the rest (vertical bars in Fig. 8). Samples containing progressively more dickite do not show any consistent change in the shape of their particle dimension distribution (vertical bars in Fig. 8). The comparison of the average sizes of Kaol 17 with the final values of the correlations for the North Sea samples (Fig. 8) indicates that the average thickness increases ~5 times, whereas the two measured dimensions in the ab plane increase ~3 times.

This is a preprint, the final version is subject to change, of the American Mineralogist (MSA)
Cite as Authors (Year) Title. American Mineralogist, in press.
(DOI will not work until issue is live.) DOI: http://dx.doi.org/10.2138/am.2014.4614

DISCUSSION

Changes of kaolin crystal order and polytype with burial

The present study does not include the whole range of kaolinite-dickite content in the North Sea samples, but it is documented from previous work that these samples correspond to a series of kaolinite-to-dickite transformation from pure kaolinite (Cassagnabere 1998). Our data show that two reactions take place with burial. One is the transformation of kaolinite into dickite. In this transformation, the contour of the reaction progress up to ~3,500 m (Fig. 2) is consistent with an increased reaction rate due to increased temperature with burial. The other reaction taking place is the increase of crystal order of kaolinite (and possibly also dickite). Lanson et al. (1996) noticed this reaction taking place at the first stages of the transformation and Marfil et al. (2003) observed kaolinite of high crystal order at burial depths where dickite was the dominant polytype. We argue here that the increase of kaolinite crystal order takes place throughout the whole burial sequence in parallel with transformation into dickite. This reaction is not totally evident from the North Sea samples alone in our study because they have a relatively narrow range of crystal order (Fig. 6). It is necessary to establish a comparison with some "typical" kaolinite that may represent the original kaolinite in the North Sea. In our opinion, Kaol 17 is appropriate for such purpose. The differential thermal analysis (DTA) diagram of pure kaolinite from sandstone in the French Aquitan Basin (Beaufort et al. 1998) is similar to the DTG diagram of Kaol 17, although showing an intermediate character between Kaol 17 and KGa-2, where the latter has a lower crystal order. Comparing the CSDS calculated from kaolinite peaks of Kaol 17 (as representing the original kaolinite in the North Sea sandstones) and the ELK series indicates that kaolinite crystal order increases with burial (Table 2). Thus, both kaolinite transformation into dickite and kaolinite recrystallization take place in parallel, and the latter reaction progresses so much that the CSDS of kaolinite domains at the final stages of the kaolinite-to-dickite transformation is similar to that of dickite.

561 It is of great interest that the only sample at 4,500 m does not show any progress in dickite content
562 from the samples ~1,000 m above. The reason for this may be the heterogeneous environment that
563 the samples encountered in terms of rock porosity (Lanson et al. 2002), interstitial fluid (oil versus
564 water; Lanson et al. 2002), or other variables affecting kaolinite reactivity. It is logical that porosity
565 should enhance reactions by facilitating solute transport (Hassouta et al. 1999), and Lanson et al.
566 (2002) show a broad positive correlation between rock porosity and dickite content in samples from
567 the Frøy reservoir, where our samples are from. Oil invasion has been considered as a possible
568 cause for the stop or slow-down of the kaolinite-to-dickite reaction (Lanson et al. 2002). In our
569 view, however, the fluid type (oil versus water) does not appear to control the dickite content shown
570 by Lanson et al. (2002) for the Frøy reservoir. Other variables may be relevant to the reaction.
571 However, the fact that we did not observe any progress of the transformation beyond 95% dickite in
572 any of the studied samples (Table 1), where the ELK series and the two BM samples have different
573 origin, together with the fact that two samples not included in this study showed development of
574 dickite and nacrite without disappearance of kaolinite (see results), suggests that there is an intrinsic
575 limit to the kaolinite-to-dickite transformation that corresponds to 90-95% dickite. If kaolinite
576 crystal order develops in certain grains, or domains within grains, at the same time that other
577 domains transform into dickite, towards the end of the transformation series the kaolinite domains
578 still present may be so large and stable that the transformation to dickite may not be feasible.
579
580 Cassagnabere (1998) and Lanson et al. (2002) display a few samples with 100% dickite. However,
581 these results are based on IR methods, using the overall shape of infrared features in the OH
582 stretching region (Cassagnabere 1998). Our quantification is based on XRD and uses the relative
583 intensity of several specific diagnostic kaolinite and dickite peaks. The existence of diagnostic
584 kaolinite peaks is positive proof of the presence of kaolinite. Our investigation using mid-IR
585 spectroscopy (described in another paper), which includes the analysis of features at several
586 wavelengths, showed that quantification of dickite-kaolinite becomes difficult at the dickite end,

where the composition curve bends and loses resolution, so that the exact composition cannot be ascertained.

Our suggestion that total transformation to dickite is prevented by the development of large and well-ordered kaolinite crystals is consistent with the fact that the relative stability of the pure polytype phases is very similar. First principle calculations by Sato et al. (2004) indicate differences of only 0.07-0.3 kJ/mol. Calculations of the ΔG of formation at standard conditions by Anovitz el al. (1991) indicated a difference of 1.38 kJ/mol in favor of kaolinite. Experimental determination of ΔG in the same conditions by De Ligny and Navrotsky (1999), Fialips et al. (2001), and Fialips et al. (2003) indicated stability differences between 2 and 25 kJ/mol only, also favourable to kaolinite. Whatever the driving force for kaolinite dickitization with burial (increasing temperature and/or pressure), the thermodynamic stability of both minerals is very similar. This would explain that kaolinite recrystallization takes place with burial at the same time as kaolinite transformation into dickite. As typical with clay minerals, the fact that one or the other reaction takes place depends probably of kinetic factors. In the deepest samples, the transformation of large kaolinite crystal domains into dickite does not take place, because the kaolinite domains are very stable. There is a negligible stability gain in the recrystallization of such large, stable kaolinite domains into dickite domains with similar stability.

Mechanism of kaolinite transformation into dickite in burial diagenesis

Our SEM study indicates that individual kaolin plates in booklets coalesce to generate thicker plates (Fig. 7). Other authors have found the same or similar sequence of particle morphological transformation and some or all of the textural details described here (Eherenberg et al. 1993; Ruiz Cruz and Moreno Real 1993; Hassouta et al. 1999; Lanson et al. 2002; Martin-Martin et al. 2007; De Bona et al. 2008), including different geologic settings such as diagenesis in shales (Ruiz Cruz and Reyes 1998) and hydrothermally altered volcanic tuff (Choo and Kim 2004). Many of the

kaolin plates appeared to be joined to other plates at one or several points whereas they had individual edges in large sections of their contour (Fig. 7). Thick grains were frequently seen to consist of thinner plates that were imperfectly joined (similar to Fig. 7f, although this specific photograph corresponds to a sample connected to hydrothermal rather than burial origin). These observations and the increased average thickness of the kaolin particles are coherent with particle coalescence as the mechanism of grain growth. In some instances, booklets were observed to come together laterally (Fig. 7b,e) making also possible that they coalesce in this direction. This process is dominated by solid-state transformation because the particles are preserved as they coalesce. Dissolution of original particles, perhaps the smallest ones, and precipitation of new ones with greater crystal order is seemingly occurring (Fig. 7c), although at small scale. Very likely, dissolution-precipitation of particle edges generating smooth, more stable surfaces is also taking place. For example, the smoothness of particle faces parallel to c increases from Figure 7a,b to Figure 7d,g. Our results show that the particle morphology is not related to specific polytype, as indicated by previous authors (see introduction), because thin platelets, thick plates and blocky habits were found in the entire range of kaolinite-dickite composition (Fig. 7).

The investigation of the size of XRD coherent scattering domains is a more reliable tool than particle morphology and dimensions to assess the mechanism of kaolinite reaction because the number of domains sampled is far greater and because the SEM study can be biased by the manner of particle aggregation, image contrast, etc, which variables can alter the visibility of particles of different size and the dimensions that can be measured in specific particles. The XRD study indicates that kaolinite domains grow at the same time that kaolinite is transformed into dickite. Considering the SEM observations above, the most direct interpretation of this fact invokes a mechanism in the solid state by which (1) crystal defects are eliminated and (2) the change of polytype takes place gradually. Given the similar stability of kaolinite and dickite structures, the two processes progress in parallel, although the transformation into dickite is the most favorable

639 reaction as indicated by the fact that it reaches 90-95% of the kaolin mass. This mechanism in the
640 solid state can also explain the fact that CSDS in the c direction grows at a greater extent than
641 CSDS in the ab plane (Table 2). How this takes place can be visualized schematically. Figure 9a
642 represents a two-dimensional view of a crystal of the original kaolinite, where the lines indicate
643 defects within the crystal, and thus the rectangles correspond to coherent scattering domains. The
644 dimensions of the domains are not proportional to those measured experimentally and the sketch is
645 only intended for illustration. Figure 9b represents the crystal at a later stage, where more crystal
646 defects in the c direction have been removed than in the ab plane, generating greater CSDS growth
647 in the c direction.
648
649 Our results show that analysis of thermal dehydroxylation of kaolinite-dickite detects the
650 progressive growth of kaolin particles and not their polytype, as indicated by Wada (1965), Stoch
651 and Wacławska (1981) and Suitch (1986). The "intermediate" dehydroxylation events (~600 °C),
652 recorded between those typical for kaolinite (~550 °C) and dickite (650 °C and above), correspond
653 to progressively growing particles (Fig. 4). Beaufort et al. (1998) assigned this "intermediate"
654 dehydroxylation event to dickite of intermediate-to-low crystal order, although, they pointed out,
655 they could not detect such low-order dickite with XRD. Our results indicate that dehydroxylation at
656 intermediate temperature must include kaolinite of increasing crystal order, and it is probable that it
657 also includes dickite of intermediate crystal order. The particle size must be one of the determining
658 factors of the dehydroxylation temperature, but also the size of well ordered crystal domains within
659 particles, because crystal defects allow water molecules to travel more easily towards the particle
660 edge and decrease the dehydroxylation temperature. Thus the displacement of dehydroxylation
661 temperature to higher values is due to both, growth of particles and coherent crystal domains within
662 them. Suitch (1986) proposed that dehydroxylation of kaolin polytypes takes place instantaneously
663 for each layer. Such is the conclusion of Drits et al. (2011) for pyrophyllite also, and they indicate
664 that pressure of the water molecules separate two layers and then water escapes through this

665 interlayer. Drits et al. (2011) argue that the greater the crystals or their crystal order the more energy
666 is required to separate the layers and dehydroxylation occurs at higher temperature. Recently,
667 Zhang et al. (2010) studied in-situ dehydroxylation of several 2:1 phyllosilicates using IR and found
668 that OH^- rather than H_2O is the species that diffuses away during dehydroxylation, and that
669 molecular water only forms close to the grain surface. The diffusion of a charged species through a
670 crystal lattice is expected to be different from that of a neutral species but, whatever the species and
671 diffusion mechanism, low crystal order and small crystal size are favorable conditions for
672 dehydroxylation.
673
674 For a thorough discussion, we can examine how a mechanism of dissolution-precipitation would
675 explain the results of our study. First of all, how can kaolinite crystal order increase at the same
676 time as kaolinite is transformed (via dissolution and precipitation) into dickite? We assume that the
677 particle size and crystal order of the original kaolinite is relatively homogeneous and lower than that
678 of dickite. This is indicated by the low dehydroxylation temperature (below 600 °C) in most
679 kaolinites in sandstone and other settings (Figure 4a,b; Beaufort et al.1998; Dudek et al. 2007;
680 Brindley and Lemaitre 1987). Keokuk kaolinite is the exception (Fig. 4c). The increase of kaolinite
681 crystal order with burial would then result from dissolution of small kaolinite particles and
682 precipitation of larger particles of both kaolinite and dickite. Considering that the relative stability
683 of kaolinite and dickite is similar, this is a coherent scenario. If kaolinite dissolution was followed
684 by dickite precipitation only, it would be necessary to assume (in order to explain the increase of
685 kaolinite CSDS) that the original particle size and CSDS distribution of kaolinite involved large
686 values, so that as the smaller particles dissolved and generated dickite only the larger kaolinite
687 particles remained. However, this would require the presence of very large particles and crystal
688 domains in the original kaolinite, such as in Keokuk kaolinite (Figs. 4c, 8), which is not apparent
689 from the thermal analysis of most kaolinites.
690

If dickite and increasingly ordered kaolinite precipitate from solution during burial it would be expected that the crystal growth of both phases is coherent in all crystallographic directions, i.e., if the average defect-free distance in each direction in the growing crystals is d_a, d_b and d_c, the volume within these defect-free vectors should also be defect-free. The calculations of the dimensions of coherent scattering domains involving ab, bc and abc crystallographic directions indicate that there is homogeneous growth in the a and b directions, but not in directions involving both c and the ab plane (Table 2). This fact indicates that crystal domains are not perfect within the volume defined by the average experimental dimensions in the individual a, b and c directions. Rather, there are crystal defects within this volume that decrease the size of CSDS in directions that include both the c direction and the ab plane. In other words, there is no correspondence between the crystal domains in the c direction and the ab plane. This is not likely to occur in crystals growing from solution, but suggests that the growth of the crystal domains in the c direction and the ab plane are taking place independently. Such an independent growth can be easily explained in a mechanism of recrystallization in the solid state. The progressive orientation of layers in a perfectly parallel position (increase of CSDS in the c direction) may occur independently, and thus in different places, from the healing of crystal defects across the ab plane in existing layers. Thus the a, b and c dimensions all grow, but not coherently as it would be expected from crystallization from solution.

The comparison of Kaol 17 with the deepest samples in the North Sea series shows that the relative growth of the particle thickness and the X-ray CSDS in the c direction are both larger than the corresponding values in the ab plane. The growth of c relative to ab for particle dimension is ~5/3 (Fig. 8) and that for CSDS is ~150% / 40% (Table 2). These two are phenomena occurring at very different scale but if they are produced by the coalescence of both layers and particles in the basal and lateral dimensions driven by the same mechanism, it can be expected that the two phenomena have similar manifestations in the several spatial dimensions.

Our interpretation is in good agreement with that of Ruiz Cruz and Moreno Real (1993) from their XRD analysis of mudstone and sandstone in the Spanish Betic Cordilleras. They concluded that (1) both kaolinite and dickite have both high crystal order and (2) they coexist within crystals in some sort of interstratified structure. The recrystallization of kaolinite and its transformation into dickite in the solid state that we describe is likely to generate such structural features. Besides structural investigation, isotope studies of kaolinite-dickite transformation series should be a powerful tool to investigate the transformation mechanism, although interpretations are frequently complicated by the difficulty to ascertain the composition of ancient and possibly mixing fluids. A number of works contain isotope data that report little or no isotope resetting in the kaolinite-to-dickite transformation (Franks et al. 1997; Parnell et al. 2000) or dickite indicating improbably low formation temperature (85-95 °C from Ruiz Cruz and Reyes 1998; 5-45 °C from Veniale et al. 2002; 50 °C from Simeone et al. 2005; 70-90 °C from Marfil et al. 2003; 50-80 °C from Osborne et al. 1994). Without engaging into the detailed discussion of the individual studies, we suggest that the preservation of much of the original kaolinite structure in dickite could be a key factor producing these results.

IMPLICATIONS

Our study shows that kaolinite transformation into dickite by burial diagenesis is substantially a defect-healing process, where crystals become more ordered, progressively larger, and the polytype changes. Thus, the reaction should have limited geochemical effects on the surrounding rock because no large amounts of solutes are released and there is no large increase in porosity due to grain dissolution. However, it is expected that kaolin diagenesis will tend to increase rock porosity to a certain extent due the coalescence of smaller into larger particles, with lower surface area, although this change in the fabric may not effectively alter porosity if it is overcome by the increasing pressure and chemical compaction due to other processes. Permeability increase with increasing relative dickite:kaolinite content between different rocks or sites of similar lithology may

be the result of other factors or due to the inverse relation, i.e., greater permeability propitiates a faster transformation from kaolinite into dickite.

ACKNOWLEDGMENTS

C. Fialips, D. Beaufort and S. Hillier are thanked for kindly providing the North Sea kaolinite-dickite series samples and the Keokuk kaolinite. C. Fialips is also thanked for discussion from the early inception of the study to the stage of data interpretation. R.V. and A.T. were funded by the Erasmus program of the EU via the University of Huelva, Spain.

REFERENCES

Anovitz, L.M., Perkins, D., and Essene, E.J. (1991) Metastability in near-surface rocks in the system Al_2O_3-SiO_2-H_2O. Clays and Clay Minerals, 39, 225–233.

Bailey, S.W. (1980) Structures of layer silicates. In G.W. Brindley and G.Brown, Eds., Crystal Structures of Clay Minerals and their X-Ray Identification, p. 1-124. Mineralogical Society, London, UK.

Beaufort, D., Cassangnabère, A., Petit, S., Lanson, B., Berger, G., Lacharpagne, J.C., and Johansen, H. (1998) Kaolinite to Dickite reaction in sandstone reservoirs. Clay Minerals, 33, 297-316.

Brindley, G.W. and Lemaitre, J. (1987) Thermal, oxidation, and reduction reactions of clay minerals. In A.C.D. Newman, Ed., Chemistry of Clays and Clay Minerals, p. 319-370. Mineralogical Society-Longman Scientific & Technical, London, UK.

Brindley, G.W., Kao, C.-C., Harrison, J.L., Lipsicas, M., and Raythatha, R. (1986) Relation between structural disorder and other characteristics of kaolinites and dickites. Clays and Clay Minerals, 34, 239-249.

Buatier, M., Travé, A., Labaume, P., Potdevin, J.L. (1997) Dickite related to fluid-sediment interaction and deformation in Pyrenean thrust-fault zones. European Journal of Mineralogy, 9, 875-88.

777 Cassagnabère, A. (1998) Caracterisation et interpretation de la transition kaolinite-dickite dans les
778 reservoirs a hydrocarbures de Froy et Rind (Mer du Nord), Norvege. PhD thesis, University of
779 Poitiers, France.
780
781 Choo, C.O., Kim, S.J. (2004) Dickite and other kaolin polymorphs from an Al-rich clay deposit
782 formed in volcanic tuff, southeastern Korea. Clays and Clay Minerals, 52, 749-759.
783
784 De Bona, J., Dani, N., Ketzer, J.M., De Ros, L.F. (2008) Dickite in shallow oil reservoirs from
785 Reconcavo Basin, Brazil: diagenetic implications for basin evolution. Clay Minerals, 43, 213-233.
786
787 De Ligny, D. and Navrotsky, A. (1999) Energetics of kaolin polymorphs. American
788 Mineralogist, 84, 506–516.
789
790 Drits, V., Derkowski, A., McCarty, D. (2011) New insight into the structural transformation of
791 partially dehydroxylated pyrophyllite. American Mineralogist, 96, 153-171.
792
793 Dudek, T., Cuadros, J., and Huertas, J. (2007) Structure of mixed-layer kaolinite-smectite and
794 smectite-to-kaolinite transformation mechanism from synthesis experiments. American
795 Mineralogist, 92, 179-192.
796
797 Ehrenberg, S., Aagaard, P., Wilson, M.J., Fraser, A.R., Duthie, D.M.L. (1993) Depth-dependent
798 transformation of kaolinite to dickite in sandstones of the Norwegian continental shelf. Clay
799 Minerals, 28, 325-352.
800
801 Fialips, C.-I., Majzlan, J., Beaufort, D., and Navrotsky, A. (2003) New thermochemical evidence on
802 the stability of dickite vs. kaolinite. American Mineralogist, 88, 837-845.

Fialips, C.I., Navrotsky, A., and Petit, S. (2001) Crystal properties and energetics of synthetic kaolinite. American Mineralogist, 86, 304–311.

Franks, S., Hameg, A., and Liang, L. (1997) Diagenetic evolution of Cambrian sandstones, Hassi Bir Rekaiz area, Algeria. American Association of Petroleum Geologists Annual Convention, 6, 37.

Goemaere, E. (2004) Dickite and nacrite from the Liege coal basin (Belgian Coal Measures Group, Westphalian, Upper Carboniferous). Geologica Belgica, 7, 285-311.

Hassouta, L., Buatier, M., Potdevin, J.-L., Liewig, N. (1999) Clay diagenesis in the sandstone reservoir of the Ellon Field (Alwyn, North Sea). Clays and Clay Minerals, 47, 269-285.

Hayes, J.B. (1936) Kaolinite from Warsaw geodes, Keokuk Region, Iowa. Iowa Academy of Sciences Proceedings, 70, 261-272.

Johnston, C.T., Kogel, J.E., Bish, D.L., Kogure, T., Murray, H. (2008) Low-temperature FTIR study of kaolin-group minerals. Clays and Clay Minerals, 56, 470-485.

Kerr, P.F. and Kulp, J.L. (1949) References clay localities – United States. In American Petroleum Institute, Project 49, Clay Mineral Standards, Preliminary Report no. 2, p. 24-25. Columbia University, New York, USA.

Kogure, T. and Inoue, A. (2005a) Determination of defect structures in kaolin minerals by high-resolution transmission electron microscopy (HRTEM). American Mineralogist, 90, 85-89.

Kogure, T., Inoue, A. (2005b) Stacking defects and long-period polytypes in kaolin minerals from a hydrothermal deposit. European Journal of Mineralogy, 17, 465-473.

Kogure, T., Inoue, A., and Beaufort, D. (2005) Polytype and morphology analyses of kaolin minerals by electron back-scattered diffraction. Clays and Clay Minerals, 53, 201-210.

Kogure, T., Elzea-Kogel, J., Johnston, C.T., and Bish, D.L. (2010) Stacking order in a sedimentary kaolinite. Clays and Clay Minerals, 58, 62-71.

Kumeda, J., Beaufort, D., and Kogure, T. (2007) Morphological features of kaolin minerals during kaolinite-to-dickite transition; FIB-TEM analyses. Euroclay 2007, Aveiro, Portugal, 22-27 July. Book of abstracts, p. 123.

Lanson. B., Beaufort, D., Berger, G., Bauer, A., Cassagnabère, A., Meunier, A. (2002) Authigenic kaolin and illitic minerals during burial diagenesis of sandstones: a review.Clay Minerals, 37, 1-22.

Lanson, B., Beaufort, D., Berger, G., Baradat, J., and Lacharpagne, J.-C. (1996) Illitization of diagenetic kaolinite-to-dickite conversion series: late-stage diagenesis of the lower Permian Rotliegend sandstone reservoir, offshore of The Netherlands. Journal of Sedimentary Research, 66, 501-518.

Lindberg, J.D. and Smith, M.S. (1974) Visible and near infrared absorption coefficients of kaolinite and related clays. American mineralogist, 59, 274-279.

McAculay, G.E., Burley, S.D., Fallick, A.E., and Kusznir, N.J. (1994) Palaeohydrodinamic fluid flow regimes during diagenesis of the Brent Group in the Hutton-NW Hutton reservoirs: constraints

855 from oxygen isotope studies of authigenic kaolin and reverse flexural modelling. Clay Minerals, 29,
856 609-626.
857
858 Marfil, R., Delgado, A., Rossi, C., La Iglesia, A., and Ramseyer, K. (2003) Origin and diagenetic
859 evolution of kaolin in reservoir sandstones and associated shales of the Jurassic and Cretaceous,
860 Salam Field, Western Desert (Egypt). International Association of Sedimentologists Special
861 Publication, 34, 319-342.
862
863 Martin-Martin, J.D., Gomez-Gras, D., Sanfeliú, T., Thiry, M., Ruiz-Cruz, M.D., and Franco, F.
864 (2007) Extensive dickitization of the Permo-Triassic fluvial sandstones from the eastern Iberian
865 Range, Spain. Clays and Clay Minerals, 55, 481-490.
866
867 Moll, W., Jr (2001) Baseline studies of the clay minerals society source clays: Geological origin.
868 Clays and Clay Minerals, 49, 374-380.
869
870 Osborne, M., Haszeldine R.S., and Fallick, A.E. (1994) Variation in kaolinite morphology with
871 growth temperature in isotopically mixed pore-fluids, Brent group, UK North Sea. Clay Minerals,
872 29, 591-608.
873
874 Palinkas, S.S., Sostarik, S.B., Bermanec, V., Palinkas, L., Prochaska, W., Furic, K., and Smajlovic,
875 J. (2009) Dickite and kaolinite in the Pb-Zn-Ag sulphide deposits of northern Kosovo (Trepca and
876 Crnac). Clay Minerals, 44, 67-79.
877
878 Parnell, J., Baron, M., and Boyce, A. (2000) Controls on kaolinite and dickite distribution, Highland
879 Boundary Fault Zone, Scotland and Northern Ireland. Journal of the Geological Society, London,
880 157, 635-640.

Parnell, J., Watt, G., Chen, H., Wycherley, H., Boyce, A., Elmore, D., Blumstein, R., Engel, M., and Green, P. (2004) Kaolin polytype evidence for a hot-fluid pulse along Caledonian thrusts during rifting of the European Margin. Mineralogical Magazine, 68, 419-432.

Ruiz Cruz, M.D. and Moreno Real, L. (1993) Diagenetic kaolinite/dickite (Betic cordilleras, Spain). Clays and Clay Minerals, 41, 570-579.

Ruiz Cruz, M.D. and Reyes, E. (1998) Kaolinite and dickite formation during shale diagenesis: isotopic data. Applied Geochemistry, 13, 95-104.

Sato, H., Ono, K., Johnston, C., and Yamagishi, A. (2004) First-principle study of polytype structures of 1:1 dioctahedral phyllosilicates. American Mineralogist, 89, 1581-1585.

Shutov, V.D., Aleksandrova, A.V., and Losievskaya, S.A. (1970) Genetic interpretation of the polymorphism of the kaolinite group in sedimentary rocks. Sedimentology, 15, 53-68.

Simeone, R., Dilles, J.H., Padalino, G., and Palomba, M. (2005) Mineralogical and stable isotope studies of kaolin deposits: shallow epithermal systems of western Sardinia, Italy. Economic Geology, 100, 115-130.

Stoch, L. and Wacławska, I. (1981) Dehydroxylation of kaolinite group minerals. I. Kinetics of dehydroxylation of kaolinite and halloysite. Journal of Thermal Analysis, 20, 291-304.

Suitch, P.R. (1986) Mechanism for the dehydroxylation of kaolinite, dickite, and nacrite from room temperature to 455°C. Journal of the American Ceramic Society, 69, 61-65.

907

908 Veniale, F., Delgado, A., Marinoni, L., and Setti, M. (2002) Dickite genesis in the 'varicoloured'
909 clay-shale formation of the Italian Apennines: an isotopic approach. Clay Minerals, 37, 255-266.

910

911 Wada, K. (1965) Intercalation of water in kaolin minerals. American Mineralogist, 50, 924-941.

912

913 Zhang, M., Redfern, S., Salje, E., Carpenter, M., and Wang, L. (2010) H_2O and dehydroxylation of
914 phyllosilicates: An infrared spectroscopy study. American Mineralogist, 95, 1686-1693.

915

916 Zimmerle, W. and Rösch, H. (1990) Petrogenetic significance of dickite in European sedimentary
917 rocks. Zbl. Geol. Paläont. Teil I, 1175-1196.

918

919 Zotov, A., Mukhamet-Galeev, A., and Schott, J. (1998) An experimental study of kaolinite and
920 dickite relative stability at 150-300 ºC and the thermodynamic properties of dickite. American
921 Mineralogist, 83, 516-524.

922

923

924

925

926

927 Table 1. Depth of the studied samples from the North Sea (ELK series), percent dickite from XRD,

928 and the standard deviation (2σ) of percent dickite.

Sample	Depth (m)	% Dickite	St. dev.
KGa-2		0	
Kaol 17		0	
Keokuk		0	
ELK 76	3036.8	42	16
ELK 33	3155.0	67	15
ELK 9	3219.9	91	2
ELK 22	3221.4	92	5
ELK 43	3256.0	72	8
ELK 5	3271.4	83	5
ELK 67	3354.1	86	8
ELK 84	3404.6	89	2
ELK 11	3415.1	90	5
ELK 63	3441.7	84	10
ELK 88	3463.1	90	2
ELK 53	3585.6	94	7
ELK 91	4519.2	93	6
BM 1923		92	10
BM 1927		89	7

Table 2. Analysis of the CSDS of several kaolinite (K) and dickite (D) XRD peaks in Kaol 17 (K initial) and in kaolinite-dickite samples with >80% dickite. K+D values correspond to peaks where kaolinite and dickite peaks coincide and they could not be deconvolved. K and D values are kaolinite and dickite peaks that could be deconvolved and measured separately. CSDS measurements from reflections within the same plane (*00l* and *0k0*) are averaged for each individual type of measurement (K, D and K+D). The standard deviation is 1σ. Growth is calculated as (CSDS-$CSDS_{K\ initial}$)×100 / $CSDS_{K\ initial}$. The calculated values follow the model explained in the text.

Experimental							Calculated			
hkl	data type	CSDS (Å)	n. of data	Stand. dev.	Growth (%)		Dimen-sion	data type	CSDS (Å)	Growth (%)
[001]	K initial	373	1							
[001]	K+D	649	12	77						
[003]	K initial	391	1							
[003]	K	1063	12	110						
[003]	D	888	12	150						
[004]	K initial	308	1							
[004]	K	890	12	107						
[004]	D	903	12	105						
[005]	K initial	300	1							
[005]	K	756	7	67						
[005]	D	761	8	132						
Aver [*00l*]	K initial	343	3	50						
Aver [*00l*]	K+D	649	1		89					
Aver [*00l*]	K	903	3	154	163					
Aver [*00l*]	D	851	3	78	148					
[020]	K initial	527	1							
[020]	K	740	5	211						
[020]	D	653	5	26						
[060]	K initial	256	1							
Aver [0k0]	K initial	391	2	191						
Aver [0k0]	K	740	1		89					
Aver [0k0]	D	653	1		67					
[200]	K initial	331	1							
[200]	D	430	12	57	30					
[110]	K+D	570	11	66			ab	K+D	512	
[130]	K+D	470	10	66						
[021]	K initial	362	1				bc	K initial	520	
[021]	K	491	2	46	36		bc	K	1120	115
[021]	D	498	12	73	38		bc	D	1120	115
[022]	K initial	222	1							
[022]	D	525	12	88	137					
[02-1]	K initial	306	1							
[024]	D	450	12	72						
[026]	D	338	5	121						
[1-1-1]	K initial	399	1				abc	K initial	581	
[1-1-1]	K+D	528	8	47	32		abc	K	1132	95
[1-1-1]	K	547	4	75	37		abc	D	1132	95
[1-1-2]	K+D	439	8	62						
[13-3]	K initial	382	1							
[26-2]	K initial	281	1							
[13-1]	K initial	437	1							
[13-1]	K	470	11	63	8					
[131]	K initial	327	1							
[131]	K	494	2	94	51					
[13-5]	K initial	228	1							
[111]	D	525	9	87						
[112]	D	476	12	70						
[113]	D	464	9	57						

Figures

Figure 1. XRD patterns of three samples, indicating the dickite content (% D). Panels a) and b) display the two samples with the highest proportion of non-kaolin phases. The identification of peaks is not exhaustive, and shows only the most prominent peaks corresponding to non-kaolin phases. c) Shows the 11 groups of peaks that were used for kaolin polytype quantification. D = dickite, K = kaolinite, Ch = chlorite, M = mica, Q = quartz, Exp = expandable phase (~11.36 Å; probably illite-rich illite-vermiculite mixed-layer), J = jarosite, Cr = crandallite, Py = pyrite/marcasite.

Figure 2. Increase of dickite abundance in the ELK series with depth. The equation (see text) is a best fit for the data points.

Figure 3. Relative intensity (as percent) of several non-basal peaks with respect to the average intensity of the 001 and 002 peaks (% intensity = $100 \times h_{non\text{-}basal} / [(h_{7.15Å} + h_{3.57Å})/2]$) of all the samples in this study, plotted versus (a) the proportion of dickite and (b) versus the coherent scattering domain size (CSDS) from the 001 peak (in Å). The regression in (b) includes all data points. The hkl indices of the peaks (different for kaolinite and dickite) are: 4.45 Å: 020, 11-1; 2.56 Å: 1-30, 20-1, 130, 20-2; 1.488 Å: 060, 33-1, 3-3-1, 33-2.

Figure 4. Thermogravimetry (TG) plots and their derivative (DTG) of selected samples: three kaolinites (a-c) and one dickite-rich specimen (d) for comparison; and four specimens from the North Sea sandstone (e-h).

Figure 5. Examples of the decomposition of the DTG diagrams in individual dehydroxylation components. The actual components may not be symmetric but this procedure allows the

962 quantification of hydroxyl loss at several temperatures. The location of the individual maxima from
963 left to right is the following: a) 509, 546, 609, 650 (arrow indicates the position of this small
964 component), 685 ºC; b) 502, 540, 610, 639, 676, 726 ºC (the small component at ~420 ºC is not
965 considered to correspond to kaolin dehydroxylation); c) 497, 535, 608, 632, 660, 675, 724 ºC.
966
967 Figure 6. a) Plot of the sum of areas (normalized to 100) of individual contributions to
968 dehydroxylation above 550 ºC, from the DTG diagrams, versus CSDS measured on the 001 peaks.
969 The full line corresponds to a regression including Keokuk; the dash line corresponds to a
970 regression without Keokuk. b) Sum of areas below 550ºC (normalized to 100) of individual
971 contributions to dehydroxylation versus the CSDS measured at the base of the 001 peak (bottom
972 quarter of peak height), in which part of the peak the contribution of small crystal domains is
973 greatest.
974
975 Figure 7. SEM images of several kaolinite and kaolinite-dickite samples. a) Kaol 17; typical
976 kaolinite booklet with plates of different thickness and signs of joining between plates. b) Keokuk
977 kaolinite; booklets with thick plates coming together in their basal and lateral faces. c) ELK 76
978 (42% dickite); on the right, group of particles with straight edges seemingly grown from solution;
979 on the left, booklet of plates with irregular shape. d) ELK 33 (67% dickite); booklet of imperfectly
980 parallel plates that are joined in some points; the arrow shows a plate introduced between two
981 diverging ones. e) ELK 43 (72% dickite); on the right, two plate booklets have come together
982 laterally and seemingly joined (arrow). f) BM 1927 (89% dickite); large particle composed of
983 individual plates of very different thicknesses. g) ELK 76 (42% dickite); thick plate-like particles
984 with some thinner plates sandwiched between them.
985
986 Figure 8. Particle size analysis of kaolinite-dickite samples in three dimensions: longest particle
987 dimension in the ab plane (c), particle dimension in the ab plane perpendicular to the longest

dimension (b), and particle thickness (a). Data points are the average size (for the ELK series the values are connected with lines) and vertical bars are the range of size values for which Frequency ≥ Maximum frequency/5. Notice that some average values plot outside this range. The vertical bar for Kaol 17 is the wide grey line. The calculated linear correlation includes only the ELK values.

Figure 9. Sketch of (a) an original kaolinite crystal divided in XRD coherent scattering domains limited by lines, and (b) the same crystal at a later stage, where many crystal defects have disappeared, mainly those limiting the domain size in the c direction. As a result, the growth of CSDS in the c direction is greater than in the ab directions. The relative dimensions of the domain sizes in the sketch are not representative of the experimental ones.

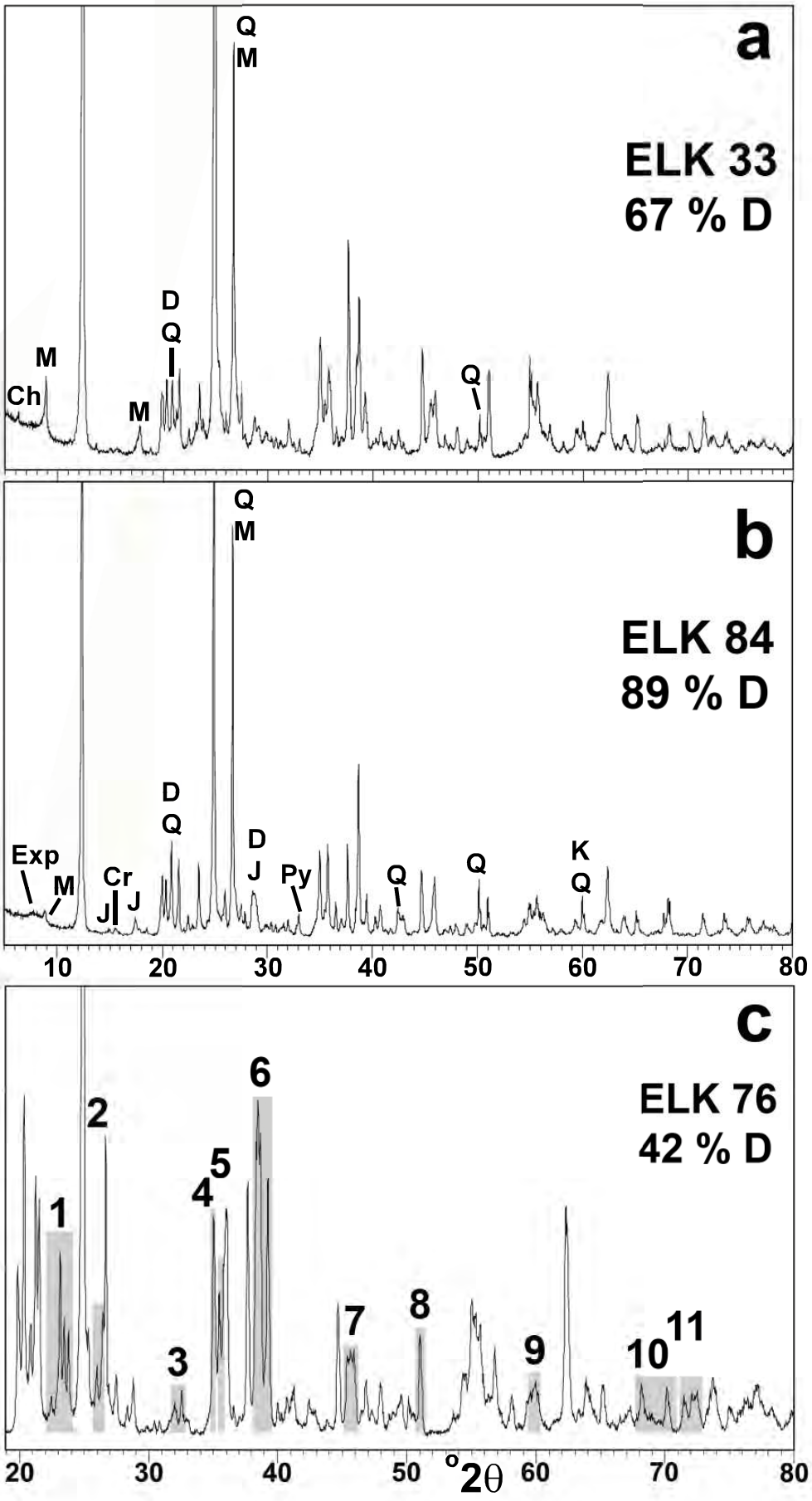
a
ELK 33
67 % D
Q
M
D
Q
M
Ch
M
Q
b
ELK 84
89 % D
Q
M
D
Q
Exp
M
Cr
J
J
D
J
Py
Q
Q
K
Q
10
20
30
40
50
60
70
80
c
ELK 76
42 % D
1
2
3
4
5
6
7
8
9
10
11
20
30
40
50
°2θ
60
70
80

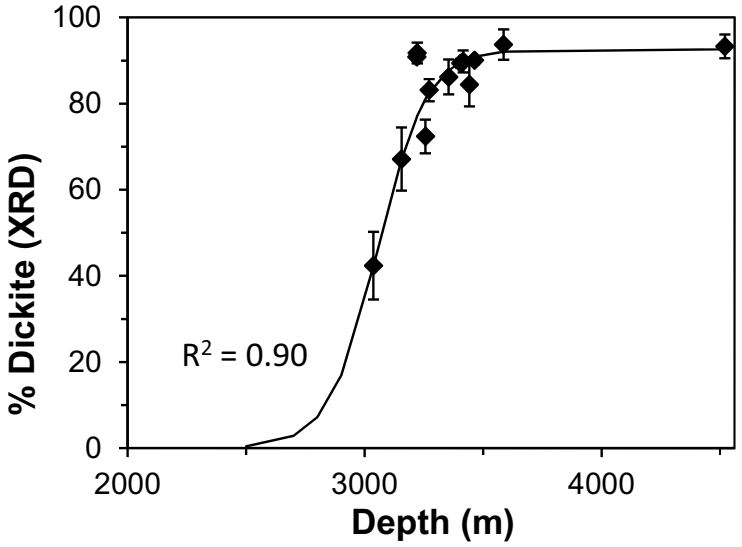

Fig. Depth (2)

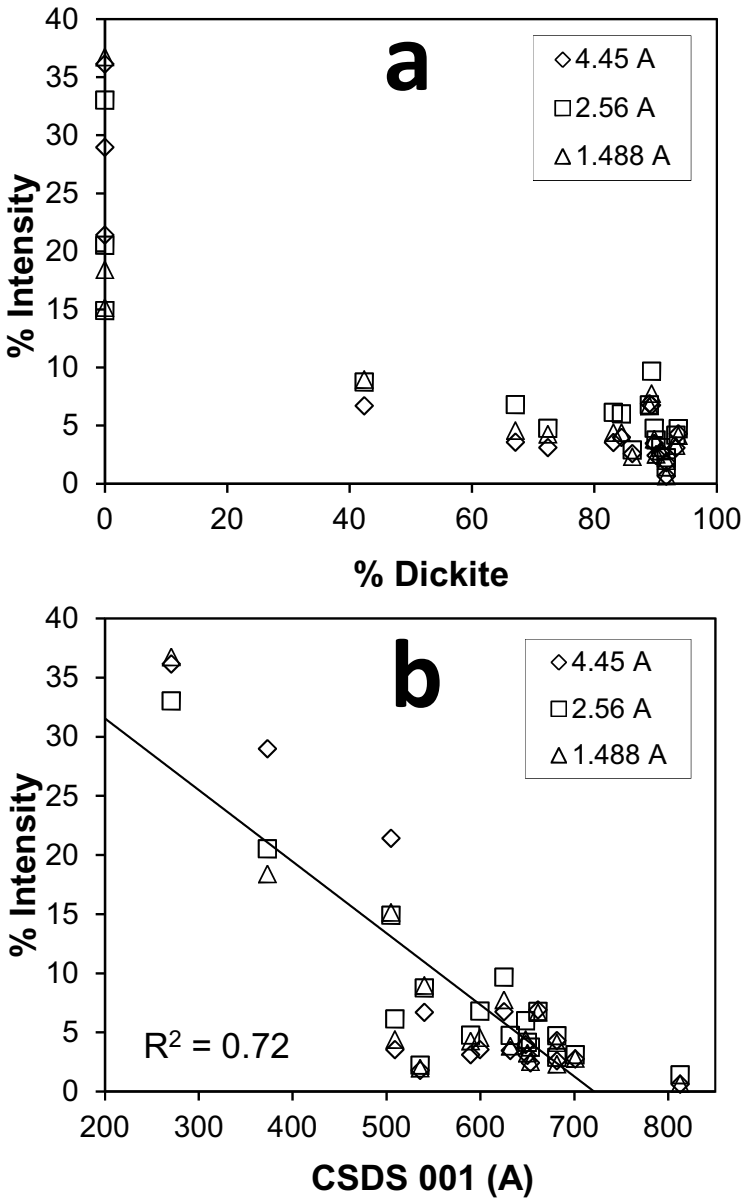
a
◇4.45 A
□2.56 A
△1.488 A
% Intensity
% Dickite
0
5
10
15
20
25
30
35
40
0
20
40
60
80
100
b
◇4.45 A
□2.56 A
△1.488 A
% Intensity
CSDS 001 (A)
R2 = 0.72
200
300
400
500
600
700
800

Fig. CSDS (3)

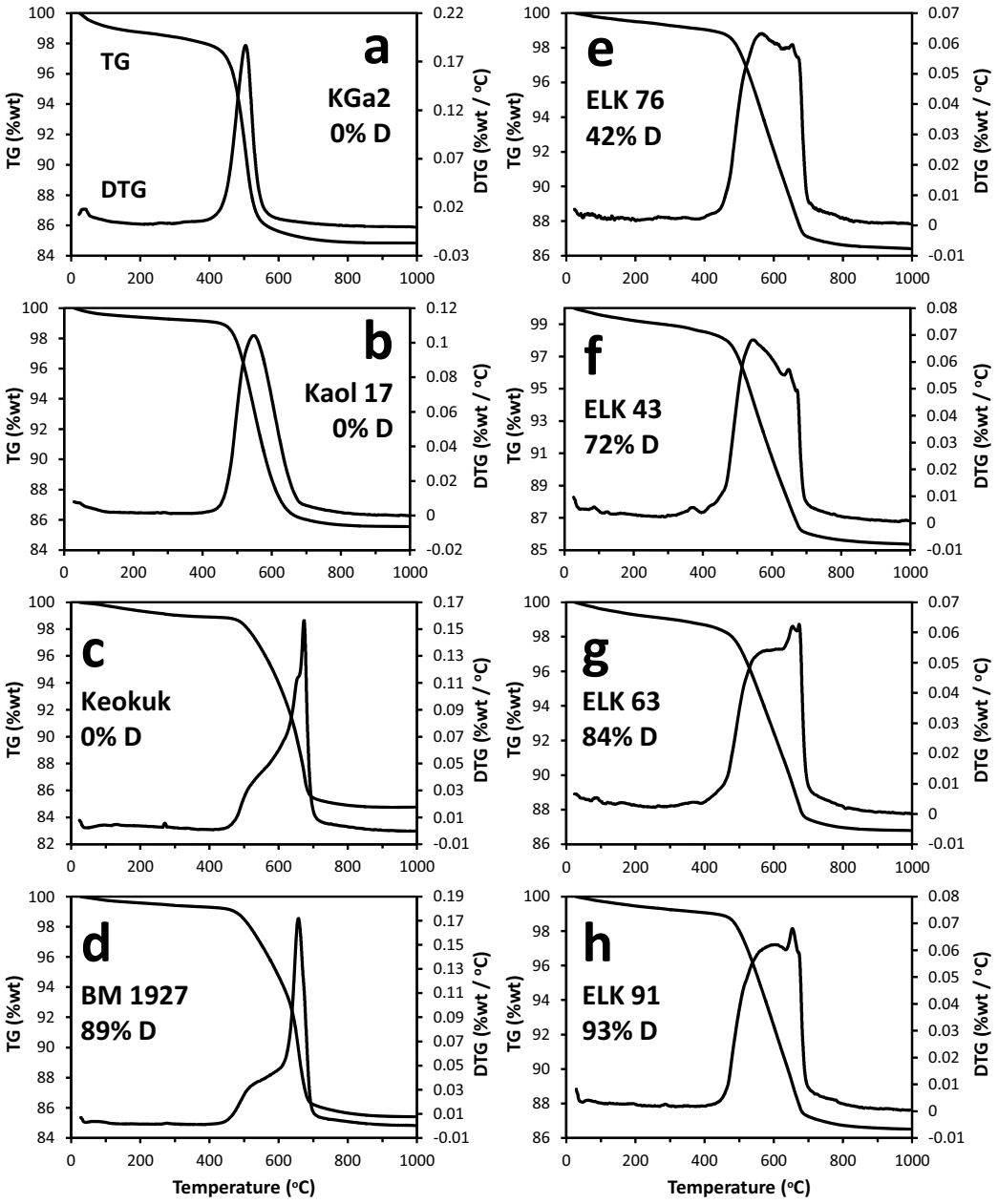
a
TG
DTG
KGa2
0% D
b
Kaol 17
0% D
c
Keokuk
0% D
d
BM 1927
89% D
e
ELK 76
42% D
f
ELK 43
72% D
g
ELK 63
84% D
h
ELK 91
93% D
TG (%wt)
DTG (%wt / °C)
Temperature (°C)

Fig TG (4)

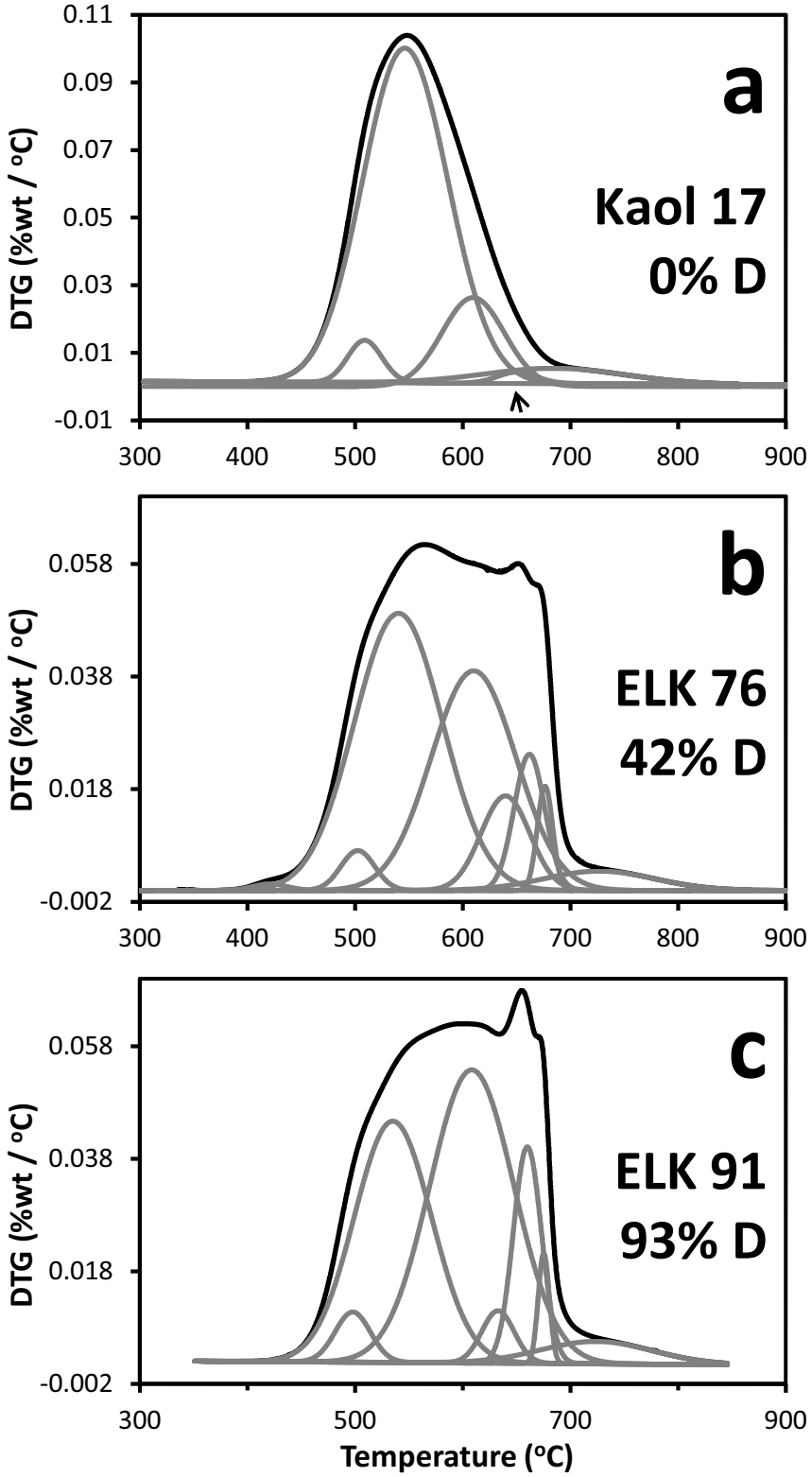
a
Kaol 17
0% D
b
ELK 76
42% D
c
ELK 91
93% D
DTG (%wt / °C)
Temperature (°C)
0.11
0.09
0.07
0.05
0.03
0.01
-0.01
0.058
0.038
0.018
-0.002
300
400
500
600
700
800
900

Fig. DTG (5)

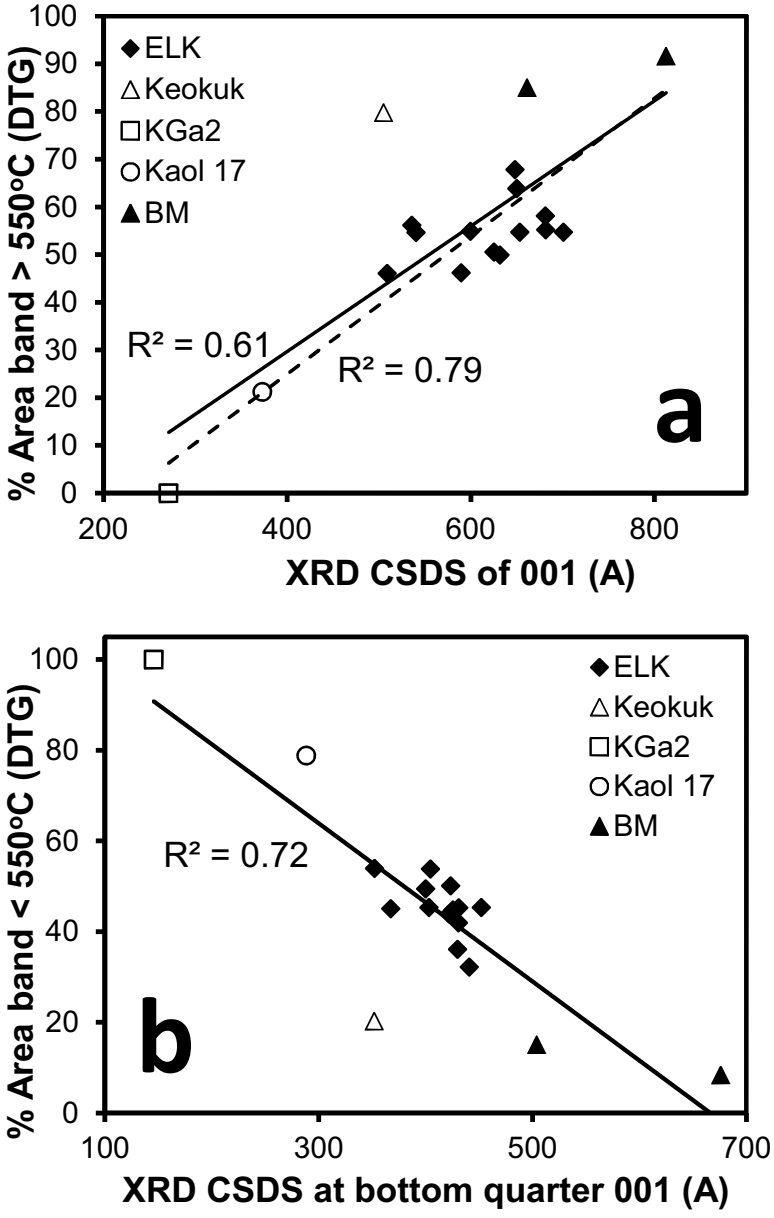
ELK
Keokuk
KGa2
Kaol 17
BM
R² = 0.61
R² = 0.79
a
% Area band > 550°C (DTG)
XRD CSDS of 001 (A)
b
R² = 0.72
% Area band < 550°C (DTG)
XRD CSDS at bottom quarter 001 (A)

Fig TGXRD (6)

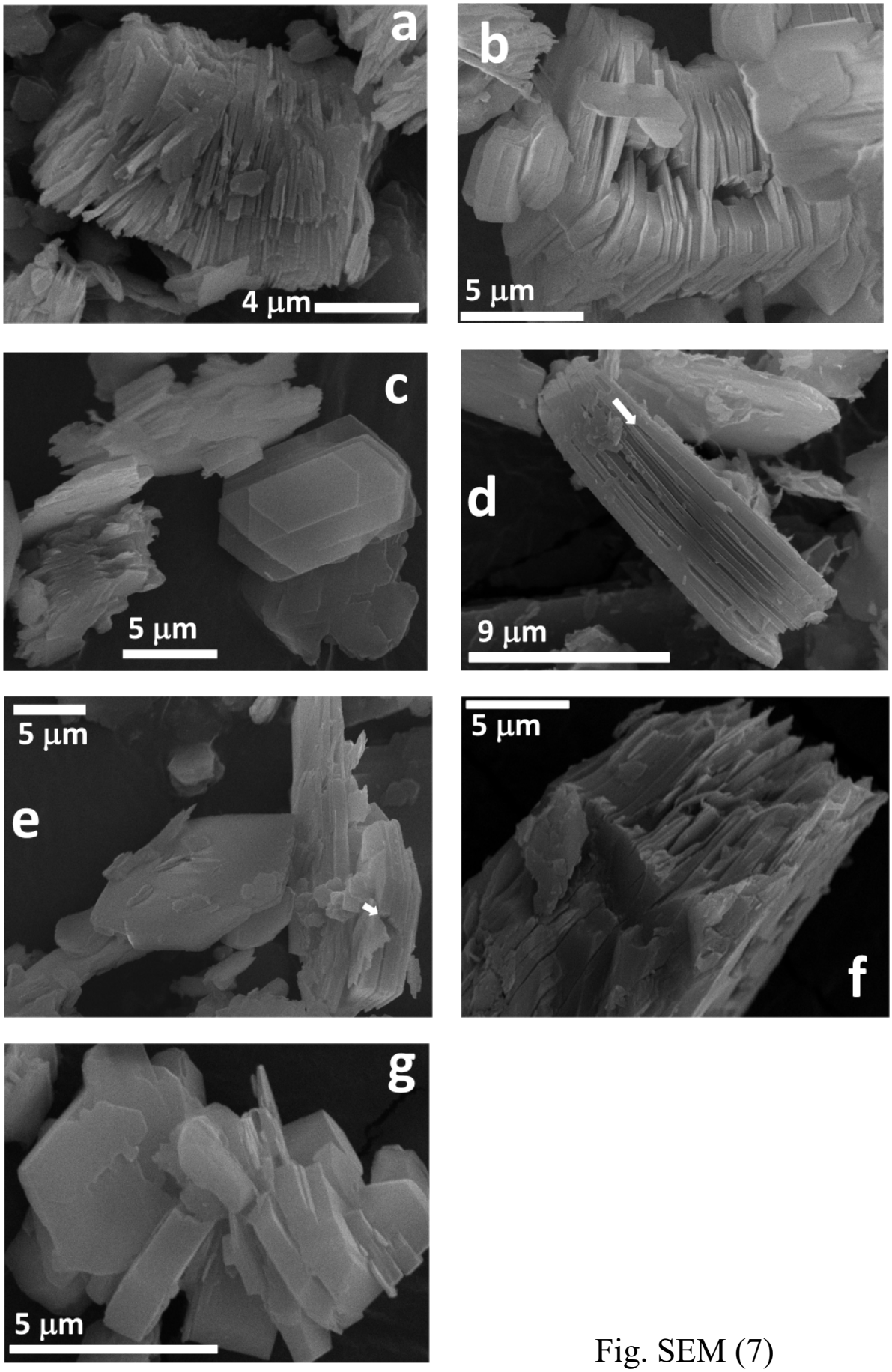

Fig. SEM (7)

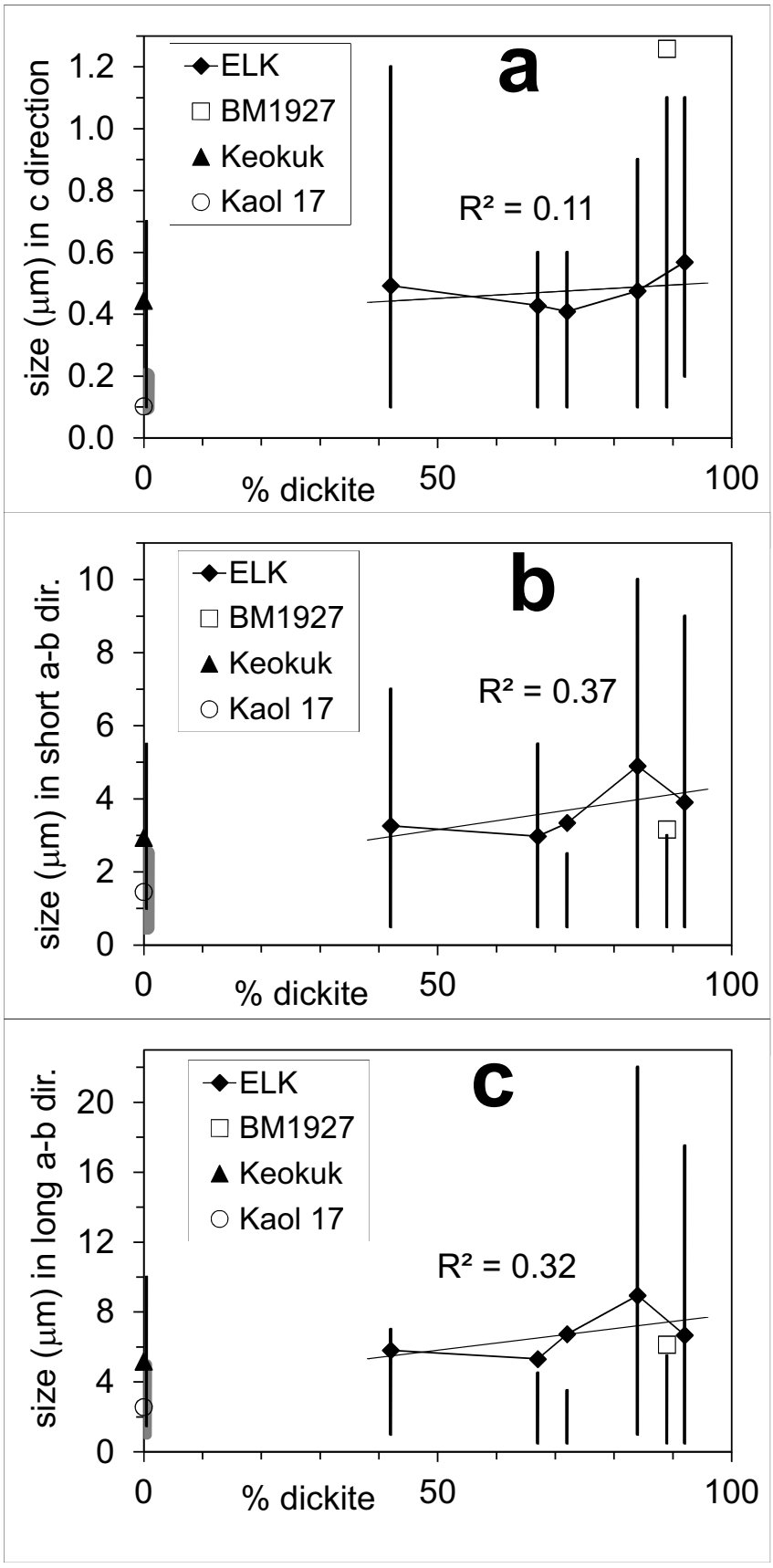
a
ELK
BM1927
Keokuk
Kaol 17
R² = 0.11
size (μm) in c direction
1.2
1.0
0.8
0.6
0.4
0.2
0.0
0
% dickite
50
100
b
ELK
BM1927
Keokuk
Kaol 17
R² = 0.37
size (μm) in short a-b dir.
10
8
6
4
2
0
0
% dickite
50
100
c
ELK
BM1927
Keokuk
Kaol 17
R² = 0.32
size (μm) in long a-b dir.
20
16
12
8
4
0
0
% dickite
50
100

Fig. DIMEN (8)

Fig Crystal (9)